

Universal Transition to Wide Shear Zones in Entangled Macroscale Chains or Ropes

M. Reza Shaebani,¹ Gerard Giménez-Ribes,² Sybren Zondervan,²
Leonard M. C. Sagis,² Erik van der Linden,² and Mehdi Habibi²

¹*Department of Theoretical Physics and Center for Biophysics,
Saarland University, 66123 Saarbrücken, Germany*

²*Laboratory of Physics and Physical Chemistry of Foods,
Wageningen University, 6708WG Wageningen, The Netherlands*

Macroscale chains have been proposed to give insight into the physics of molecular polymer systems. Nevertheless, understanding the rheological response of systems of quasi-one-dimensional semiflexible materials, such as bead-chain packings, is currently a great challenge. We study the nonlinear rheology of random assemblies of macroscale chains—including steel bead chains and cooked spaghetti—under oscillatory shear. We show that a universal transition from localized to wide shear zones occurs upon increasing the strain amplitude, for a wide range of lengths, flexibilities, and other structural parameters of the constituent elements. The critical strain amplitude coincides with the onset of strain stiffening development in the system. We obtain scaling laws for transition sharpness, shear-zone width, and stiffness enhancement as a function of chain length. Our findings suggest that the entanglements between the constituent elements strengthen when approaching the critical strain amplitude and rapidly become long range, even spanning the entire finite system for long enough chains. We show that the nonlinear rheological response is governed by the interplay between increasing stored elastic forces due to entanglements and increasing contribution of dissipation with shear rate and interlocking between chains.

Disordered assemblies of long semiflexible objects are a class of materials ubiquitously observed in nature and daily life. Examples are bird nests [1], aegagropila networks [2], and unwoven textiles [3]. An intriguing and important property of such entangled assemblies is their mechanical response and yielding when subject to external stresses. For example, packings of bead chains exhibit a striking strain stiffening under shear [4, 5]. The complexity arises from the presence of topological constraints such as (semi)loops, knots, and interlocking between the constituent elements [5–11]. The behavior differs considerably from that of packings of rodlike objects, where the physics is mainly governed by frictional interactions, volume exclusion, and aspect ratio of rods. Despite the analogies with polymeric materials [12, 13], developing a quantitative theory of stability and unjamming response of macroscale chain assemblies requires a detailed understanding of the roles of entanglements and friction, which is still lacking. The insight from the mechanical response of entangled-driven athermal systems of long semiflexible objects can guide future design of new smart unwoven textiles [14–16], knitted fabrics [17], and artificial mussels and tissues [18].

Upon yielding, slowly sheared packings of individual beads often form rigid regions separated by narrow shear zones near moving boundaries where the material flows with a shear-rate-independent profile shape [19, 20] (though wide shear zones have also been reported when shearing the bulk material away from the boundaries [21, 22]). While shear banding in frictional granular materials can be understood based on energy dissipation considerations [23, 24], much less is known about the yielding of semiflexible chain assemblies, particularly,

whether and how far entanglements and chain length and flexibility broaden the shear zones and extend them into the bulk. Since shear zones mark regions of material failure and energy dissipation, understanding the yielding behavior of chain assemblies is crucial in industrial processes and for design of new disordered meta materials [2, 3, 25, 26]. As a daily-life application, by twisting cooked spaghetti on a plate with a fork, an interesting question is how the amount of rolled spaghetti around the fork depends on length, softness, and adhesion of the strands?

The rheological response of viscoelastic materials is of fundamental importance in physics, engineering, and biology. There has been growing interest in nonlinear viscoelastic responses to large strains [27–30], e.g., to differentiate between materials with similar linear but drastically different nonlinear responses.— A highly informative protocol is to apply an oscillatory shear strain [29–31]: After many cycles to become independent of the prior history of the sample, the steady-state stress response can be probed over a wide strain range from below to above the yield point.— Nevertheless, the rheology of macroscale chain assemblies remains less explored [32]. It is unclear how the interplay between topological constraints and dissipation governs the nonlinear rheological physics of these systems.

In the present work, we study the rheological response of bead-chain assemblies to oscillatory shear deformations in experiments and numerical simulations and compare it to that of cooked spaghetti. We observe a striking universal transition from narrow shear zones at small amplitude oscillatory shear (SAOS) to wide shear zones at large amplitude oscillatory shear (LAOS). In-

ing the length of the constituent elements sharpens the transition and enhances the extent of the wide shear zone, for which power-law scaling relations are obtained. Our results show that the system undergoes a rather sharp crossover from inactive entanglements in SAOS to system-spanning activated entanglements in LAOS. We demonstrate that the nonlinear rheological physics of macroscale chain assemblies is governed by the competition between stored elastic and dissipative (viscous) forces: The applied shear strain enhances the elastic contribution to stress by strengthening the topological constraints while the contribution of dissipation—which is proportional to the shear rate—grows above the yield point and also with increasing the interlocking between the constituent elements.

Our rheometer setup shown in Fig. 1A consists of a cylindrical container of inner radius R and a rotating four-blade vane with blade radius R_v , which applies a sinusoidal deformation

$$\phi = \phi_o \sin(2\pi ft), \quad (1)$$

where ϕ is the deflection angle, and ϕ_o and $f=0.1$ Hz denote the rotation amplitude and frequency, respectively. As a model material, we use either cooked spaghetti (which is cut into equal pieces) or bead chains consisting of hollow spherical beads with diameter d flexibly connected to each other by enclosing dog-bone-shaped links. The induced gap size ℓ between the neighboring beads varies in the range $0 \leq \ell \leq \ell_{\max}$. The links also limit the local turning angle θ of the chain to $0 \leq \theta \leq \theta_{\max}$; see Fig. 1B and *Materials and Methods* section for details. An instantaneous persistence $p = \cos(\theta)$ can be assigned to the chain nodes [33] from which the local persistence length ℓ_p can be obtained via $p = e^{-\ell/\ell_p}$ [13, 34, 35]. We also perform extensive contact dynamics (CD) simulations [36] of spherical rigid beads in a setup similar to our experiments. We impose upper bounds on the distance between the centers of neighboring beads and on the angle between lines connecting three neighboring beads along the chain. This concept is suited very well to the CD method where interparticle forces are handled as constraint forces [37, 38].

Universal transition to wide shear zones

We start the experiments in the SAOS regime, i.e. with small rotation amplitudes. In this regime, the surface velocity profiles reveal that the movements diminish rapidly with increasing distance from the rotating blades, independent of the chain length N ; see e.g. the experiments at $\phi_o = 0.063$ rad in *Suppl. Movie S1*. Denoting the mean velocity at the radial coordinate r with $v(r)$, Fig. 2A shows that v decays fast with r ; a jammed immobile region is reached after 1-2 bead diameter distance. The velocity fluctuations are relatively small and the profiles are reproducible to a large extent independent of the initial conditions. Formation of narrow localized shear zones near moving boundaries was observed in quasistatic shear of granular materials [19, 20]. Here, the independence of

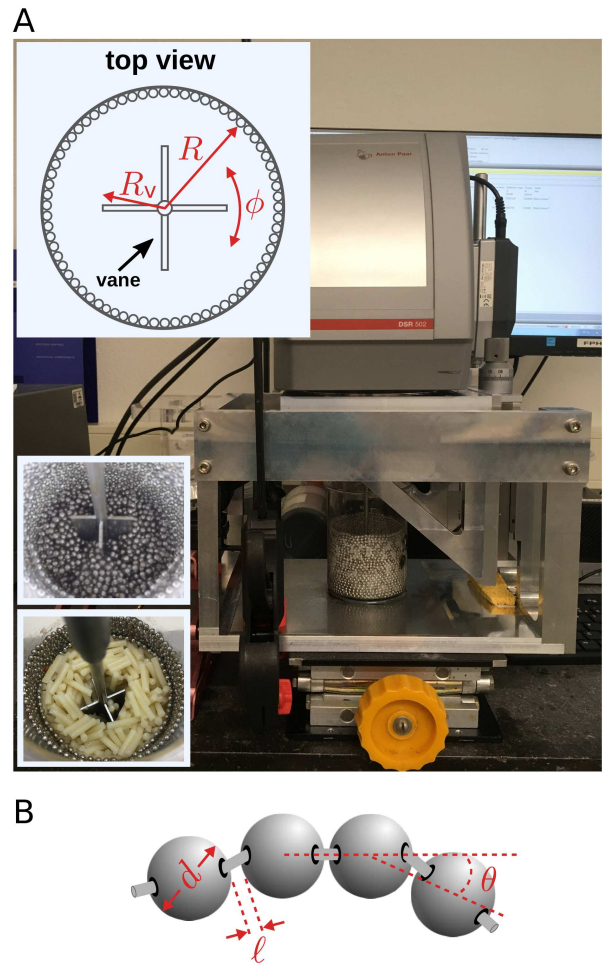


FIG. 1. **Setup and bead-chain geometries.** (A) Four-blade vane rheometer setup. Upper inset: top view of the cell, not to scale. $R_v = 11$ mm; $R \simeq 34$ mm. Lower insets: images of shear experiments with steel bead chains or cooked spaghetti. (B) Schematic of the bead chain with ℓ and θ indicating the bond length and turning angle, respectively, and $d = 2.4$ mm being the bead diameter. ℓ is variable from 0 to $\ell_{\max} = 0.4$ mm and θ from 0 to $\theta_{\max} \simeq 40^\circ$ in experiments.

the results from N indicates that the topological constraints have not been activated yet and do not play a role in the SAOS regime.

To quantify the extent of the shear zone, we assign a width r_c to the shear zone as the radial distance from the cylinder axis at which the velocity drops below a threshold value; see Fig. 2B. Here we report the results for the threshold velocity $v_c = 4 \times 10^{-5}$ m/s; however, we checked that the observed trends and our conclusions are insensitive to this choice in a moderate range of velocities.

The behavior is markedly different in the LAOS regime: The shear zone extends to the bulk of the system, as shown in Fig. 2A (see also *Suppl. Movie S1* for experiments at $\phi_o = 0.632$ rad). It was previously reported that oscillatory shear of granular materials with large amplitudes broadens the shear zone up to a few bead di-

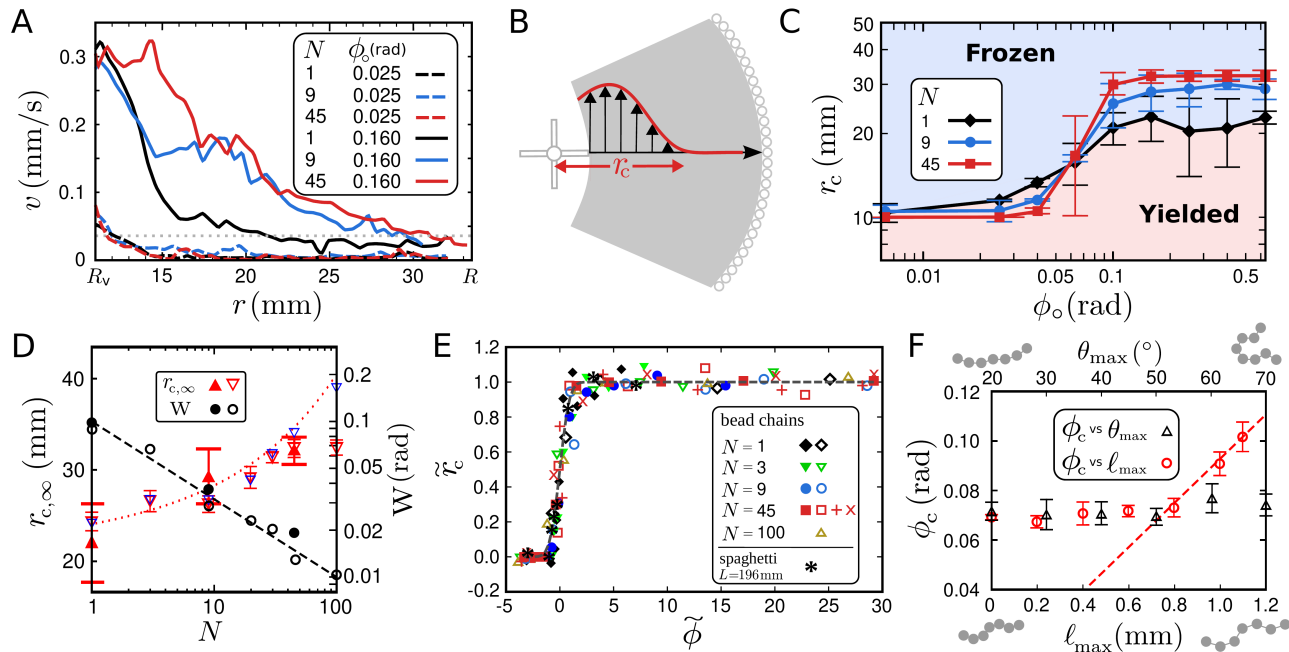


FIG. 2. **Chain dynamics in oscillatory shear.** (A) Mean bead velocity v as a function of distance r from the cylinder axis for different values of rotation amplitude ϕ_o and chain length N . The dotted line denotes the threshold velocity v_c . (B) Definition of the shear-zone width r_c . The velocity field is sketched with vertical arrows. (C) Shear-zone width r_c versus rotation amplitude ϕ_o . The yielded and frozen regions for $N=1$ are indicated with different colors. (D) Saturation width $r_{c,\infty}$ of the shear zone and transition sharpness W (indicating the range of rotation amplitudes over which the transition occurs) in terms of N . Full (open) symbols correspond to experimental (numerical) results. Blue open symbols represent the simulation results for a larger container with $R \simeq 100$ mm. The black dashed line is a fit to Eq. (2), and the red dotted line represents a growth according to Eq. (3), as a guide to the eye. (E) Collapse of all rescaled shear-zone widths $\tilde{r}_c = \frac{r_c - r_{c,0}}{r_{c,\infty} - r_{c,0}}$ as a function of rescaled rotation amplitude $\tilde{\phi} = \frac{\phi_o - \phi_c}{W}$, obtained for different chain lengths in experiments (full symbols) and simulations (open symbols). The simulation results for a chain with zero bond length $\ell_{\max} = 0$ (pluses) or high flexibility $\theta_{\max} = 70^\circ$ (crosses) at $N=45$ are also presented. The dashed line is a fit to the error function (4). (F) Transition center ϕ_c versus maximum bond length ℓ_{\max} or maximum turning angle θ_{\max} obtained from simulations for $N=45$. The line represents $\phi_c = \ell_{\max}/R_v$.

ameters, as the shear stress drops at the shear direction reversals [39]. Our notable observation is the influence of chain length on the shear deformation at large strains: With increasing N , the shear zone becomes much wider, the velocity profile strongly depends on the initial condition, and large velocity fluctuations along the radial coordinate are observed even for a single experiment.

To understand how the system crosses over from narrow shear zones in SAOS to wide system-spanning ones in LAOS, we vary systematically ϕ_o for different chain lengths and repeat the measurement for different non-consecutive cycles in each sample to smoothen the velocity fields. The width r_c of the shear zone as a function of ϕ_o is shown in Fig. 2C. Interestingly, the change of r_c when moving from the SAOS to the LAOS regime is not gradual but happens over a narrow range W of rotation amplitudes. For longer chains the transition is sharper, corresponding to a smaller W . By fitting each $r_c - \phi_o$ curve to an error function, we assign a W to it. The plot of the resulting W values in terms of N in Fig. 2D implies that W scales as

$$W \sim N^{-\alpha}, \quad (2)$$

with the exponent $\alpha \simeq 0.5$.

Figure 2C also reveals that r_c reaches a plateau level at large ϕ_o , which is higher for longer chains. Denoting this maximum shear-zone width with $r_{c,\infty}$, Fig. 2D shows that $r_{c,\infty}$ initially grows with N but gradually approaches the inner radius R of the container (full triangles). The saturation behavior at larger N is more visible in the simulation results (red open triangles). The question arises whether the shear zone for long chains can penetrate further into the bulk of the system in an infinite system (i.e. when $R \rightarrow \infty$). To answer this, we perform simulations with chain lengths up to $N=100$ and increase the container radius from $R \simeq 34$ to 67 and 100 mm. As the resulting $r_{c,\infty}$ values for the two latter system sizes are the same (within the error bars), we conclude that the shear zones for chain lengths $1 \leq N \leq 100$ cannot be wider if the system size is further increased beyond $R=100$ mm. A comparison between the results at $R=34$ (open red triangles) and $R=100$ mm (open blue triangles) in Fig. 2D shows the finite-size effects on $r_{c,\infty}$ values for longer chains. The system-size-independent width of the shear zone (blue symbols) can be approxi-

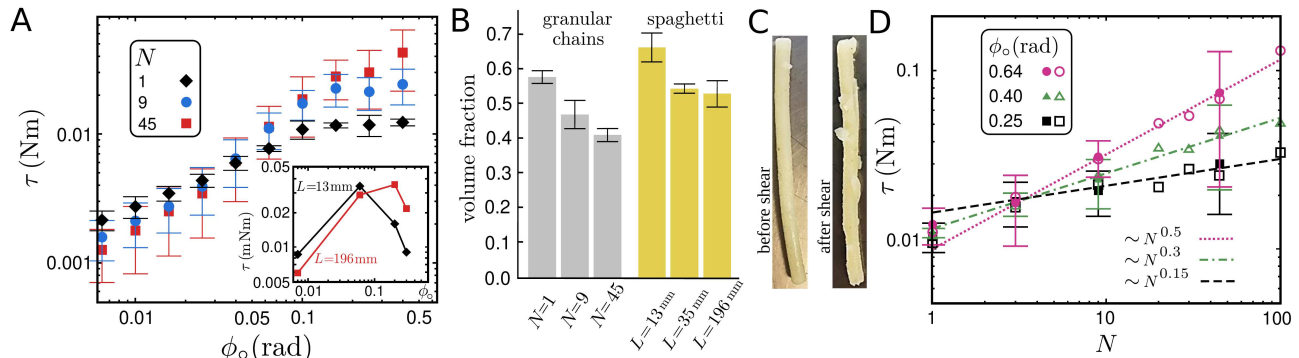


FIG. 3. **Stiffening of macroscale chains.** (A) Torque τ versus rotation amplitude ϕ_0 for different bead chain lengths. Inset: τ vs ϕ_0 in shear experiments with cooked spaghetti of length L . (B) Volume fraction of bead chain or spaghetti assemblies. (C) Example of surface roughening of spaghetti due to oscillatory shear. (D) τ versus N for different values of ϕ_0 in experiments (full symbols) and simulations (open symbols). The lines represent power-law fits to $N \geq 3$ data.

mately described by

$$r_{c,\infty}(N) - r_{c,\infty}(N=1) \sim N^\beta, \quad (3)$$

with $\beta \approx 0.5$. The radius of gyration of a flexible chain similarly scales with \sqrt{N} [34]. This suggests that in the LAOS regime the topological constraints are fully activated along the entire length of the chains that are moved by the rotating blades. As a result, their motion can influence a bulk region of size proportional to their radius of gyration, i.e., $\propto \sqrt{N}$.

Figure 2E illustrates our main result: After proper rescaling, all $r_c - \phi_0$ data collapse on a universal curve which is well fitted by an error function. We introduce the rescaled shear-zone width $\tilde{r}_c = \frac{r_c - r_{c,0}}{r_{c,\infty} - r_{c,0}}$, with $r_{c,0}$ being the minimum shear-zone width. Thus, the dimensionless number \tilde{r}_c takes values in $[0, 1]$. All rescaled shear-zone widths follow a universal master curve

$$\tilde{r}_c = \frac{1}{2} \left(1 + \operatorname{erf} \left(\frac{\phi_0 - \phi_c}{W} \right) \right), \quad (4)$$

where W is the range of amplitudes over which the transition occurs (transition width) and ϕ_c is the rotation amplitude at the center of the error function (transition center). We checked that the spaghetti data and also simulation results for $1 \leq N \leq 100$ and other values of the maximum bond length in the range $0 \leq \ell_{\max} < d/2$ or maximum turning angle in the range $20^\circ \leq \theta_{\max} < 70^\circ$ are well fitted to Eq. (4).

From the fits of $r_c - \phi_0$ curves to an error function, we find that the transition center ϕ_c does not depend on N . This can be also seen from Fig. 2C; we get $\phi_c \simeq 0.07$ rad by averaging over experiments with different N . Simulations with different values of θ_{\max} or ℓ_{\max} shown in Fig. 2F reveal that ϕ_c is independent of the chain flexibility θ_{\max} . Moreover, ϕ_c is insensitive to variation of ℓ_{\max} for small bond lengths but grows approximately linearly for $\ell_{\max} \gtrsim 0.8$ mm.

A plausible scenario is that the transition center ϕ_c is the onset at which the shearing brings the bonds

between neighboring beads to their maximum possible length ℓ_{\max} quickly after each shear direction reversal. Above this threshold rotation amplitude, the chains are in a stretched form in the absence of the internal degrees of freedom of having variable bond lengths. This would lead to the prediction $\phi_c \approx \frac{\ell_{\max}}{R_v}$, i.e. a linear increase of ϕ_c with ℓ_{\max} . Figure 2F shows that this simple model captures the behavior for long bonds. But why does not ϕ_c grow proportionally to ℓ_{\max} for short bonds? From simulations with $N=1$, we observe that a minimum rotation amplitude of the order of 0.06–0.07 rad is required to generate wide shear zones in packings of individual beads. That is why the increase of ϕ_c with ℓ_{\max} is only visible for bond lengths $\ell_{\max} \gtrsim 0.8$ mm for which $\phi_c \gtrsim 0.07$ rad.

Stiffening upon increasing strain amplitude

The crossover from narrow to wide shear zones suggests the presence of entanglements above the transition threshold ϕ_c . One of the entanglement mechanisms is the interlocking between the beads of different chains. We expect that stretching of bonds to ℓ_{\max} at ϕ_c immediately activates this type of topological constraints for all chain lengths $N \geq 3$. Formation of (semi)loops is another entanglement mechanism, which strengthens with increasing N and/or ϕ_0 above ϕ_c . Note that a full ring requires a minimum chain length $N=9$. The fact that the shear-zone width rapidly saturates above ϕ_c for all N shows that interlocking is the major entanglement mechanism affecting the flow properties of chain assemblies. Loop formation induces weak entanglements for $N < 9$ and, moreover, should lead to ϕ_0 -dependent wide shear zones which is not observed. It is however expected that semiloops play the major role in the strain stiffening phenomenon [4, 5].

As a direct proof of the activation of entanglements, we probe the mechanical response of the system upon increasing ϕ_0 . By measuring the maximum exerted torque τ by the rheometer on the system in an oscillatory shear cycle for a given rotation amplitude ϕ_0 and repeating it for different ϕ_0 values, we plot τ as a function of ϕ_0 in

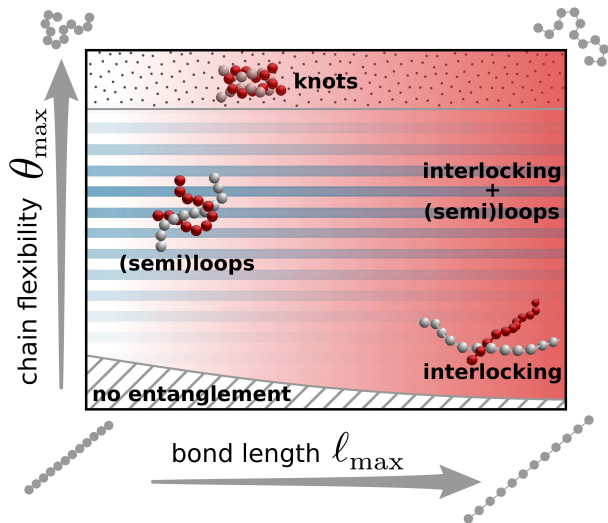


FIG. 4. **Schematic phase diagram of entanglement mechanisms at a given chain length.** The contribution of (semi)loops grows with increasing chain flexibility from rod-like chains; however, extremely flexible chains promote knot formation. Increasing bond length gradually enhances the contribution of interlocking between chains. Gradients of red and blue colors qualitatively indicate variations in the contributions of interlocking and semiloops, respectively.

Fig. 3A. In the absence of entanglements at small strains, shearing the packings of individual beads ($N=1$) requires a larger τ compared to long-chain packings, due to having a higher packing fraction; see Fig. 3B and Ref. [6] (Although packing structure strongly depends on the interparticle friction [40–42], we assume that it affects the assemblies with different N in a similar way). In contrast, at large amplitude oscillations, yielding occurs for $N=1$ while assemblies of longer chains exhibit shear stiffening. The crossover point in Fig. 3A interestingly coincides with the onset ϕ_c of the transition to wide shear zones. We observe a similar transition point and mechanical response trend in the case of spaghetti (inset of Fig. 3A), even though they cannot sustain large torques in the strain stiffening regime: Large amplitude shear of spaghetti leads to roughening of strand surfaces (Fig. 3C), cutting of strands into shorter pieces, and ascending and ordering of strands above the probe. Moreover, it was previously reported that shear rate (which increases with ϕ_o in our experiments) and interfilament overlap length enhance the sliding friction between filaments [43]. Nevertheless, observing a similar onset of stiffening for bead chains and spaghetti is striking and it possibly points to a universal mechanical response of assemblies of long semiflexible objects.

Figure 3A shows that the degree of stiffening not only depends on ϕ_o but also on N [4]. When plotting τ vs N for different ϕ_o in Fig. 3D, we find that τ scales as a power-law with the chain length (for $N \geq 3$)

$$\tau \sim N^{\gamma(\phi_o)}. \quad (5)$$

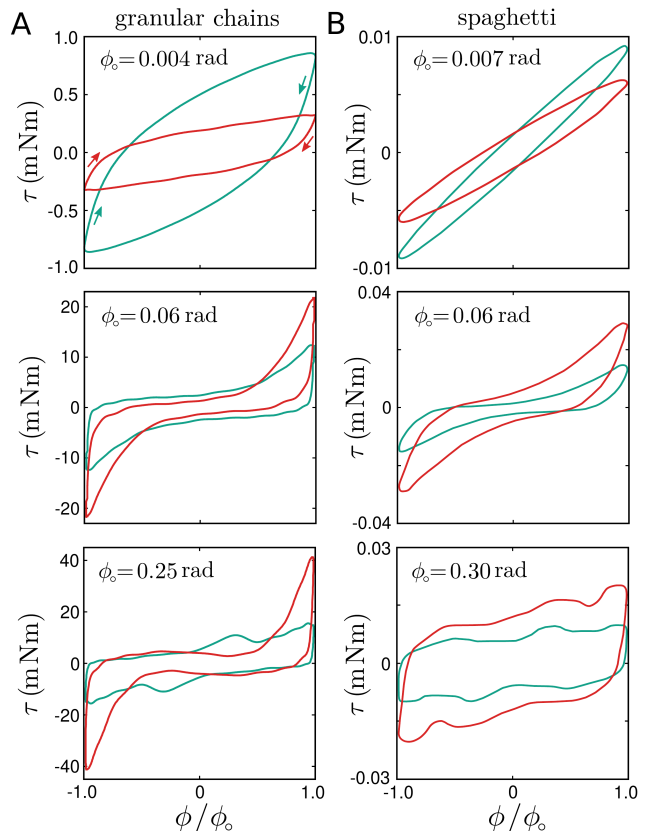


FIG. 5. **Elastic Lissajous curves of sheared bead chains and spaghetti.** (A) Lissajous plots of torque vs deflection angle ϕ (scaled by ϕ_o) for bead chains of length $N=1$ (green) and $N=45$ (red). (B) Similar plots for assemblies of spaghetti with length $L=13$ mm (green) and $L=196$ mm (red).

The exponent γ depends on ϕ_o ; it increases from $\gamma=0$ at $\phi_o=\phi_c$ and reaches, e.g., $\gamma \simeq 0.5$ at $\phi_o \simeq 0.64$ rad. By varying ℓ_{max} in simulations from 0 to $\sim d/3$ to increase the contribution of interlocking, we find a nearly 20% increase in τ , reflecting the greater contribution of semiloops to the mechanical response. For a given chain length, Fig. 4 summarizes the effective entanglement mechanisms in the $(\ell_{max}, \theta_{max})$ space, i.e. upon varying chain flexibility and interparticle bond length.

Nonlinear rheological response

To clarify the similarities and differences between the rheological response of bead-chain and spaghetti assemblies, we apply many cycles of oscillatory shear to reach the steady-state stress response. Next, we plot the torque τ and the deflection angle ϕ in one shear cycle in the form of parametric Lissajous-Bowditch curves, similar to the stress vs strain curves commonly used in the literature [44] (As the calculation of stress and strain in our inhomogeneously sheared system involves approximations, here we use raw τ - ϕ data to avoid approximation errors). In the SAOS regime (Fig. 5, top row), we observe that the spaghetti data display an ellipsoidal shape, characteristic of a linear viscoelastic response. The response

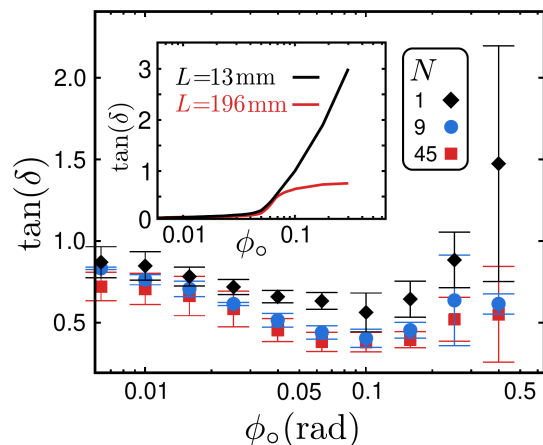


FIG. 6. **Chain-length dependence of the loss tangent.** The main panel represents the loss tangent $\tan(\delta)$ versus rotation amplitude ϕ_0 for different bead chain lengths. The inset represents a similar comparison between assemblies of spaghetti with different lengths.

of granular chains displays a rhomboidal shape. The nonlinear behavior indicates that higher harmonics are present in the signal. The degree of stiffening is larger for shorter constituent elements (being bead chains or spaghetti strands) in agreement with Fig. 3A. Around the transition amplitude ϕ_c (middle row), a highly nonlinear torque response develops in both systems, evidencing the emergence of intracycle stiffening. Here, the curves develop a larger degree of stiffening for assemblies of longer constituent elements. We also note that the stiffening in bead-chain Lissajous curves is more pronounced due to the simultaneous formation of loops and activation of interlocking; the latter is absent in spaghetti assemblies. The main difference between the rheological response of bead-chain and spaghetti assemblies arises in the LAOS regime (bottom row): In bead chains, while packings of individual beads ($N=1$) yield, assemblies of longer chains exhibit an even stronger response. In contrast, spaghetti assemblies are unable to develop higher stress and yield at all strand lengths; still, the response remains steeper for longer spaghetti strands.

Finally, we clarify how viscous stresses develop with increasing the rotation amplitude ϕ_0 in macroscale chain assemblies. This can be achieved, e.g., by analyzing viscous Lissajous curves of τ vs $\dot{\phi}$. Here, we alternatively consider the loss tangent, $\tan(\delta)$, which is a dimensionless parameter that measures the ratio of dissipated to stored energy in one cycle of oscillation. The results shown in Fig. 6 reveal that packings of individual beads dissipate a larger fraction of energy compared to chain assemblies, even in SAOS. The difference becomes more pronounced in LAOS due to the frictional flow of the yielded assemblies of individual beads as well as the increased contribution of the stored elastic energy in chain packings upon strengthening the entanglements. A similar trend is observed in shearing of spaghetti, i.e., longer strands

dissipate less energy. Here, the role of the stored elastic energy is less important since longer strands fail to develop entanglements at large shear strains. Instead, the frictional flow of shorter strands is more dissipative.

Conclusion

In conclusion, we have studied the nonlinear rheology of entangled assemblies of long semiflexible objects. Unveiling the rheological response of externally-driven interacting particle assemblies—particularly quasi-1D materials such as (bio)polymers and granular chains—is currently a great challenge for statistical physics. Our results demonstrate a universal transition from narrow shear zones at low amplitudes of oscillatory shear to broad ones at large amplitudes with a width that scales with the chain length. We have linked this intriguing rheological response to the development of topological and geometrical constraints: The system undergoes a sharp crossover from lacking entanglements to a highly entangled environment. Nevertheless, entanglements are not the only influential factor in determining the mechanical response and yielding of macroscale chain assemblies. Friction is known to play a crucial role in packings of individual beads and networks of fibres [45–47]. Understanding how the interplay of friction and entanglements governs the rheological response of chain assemblies is a future challenge toward answering the question of how assemblies of long flexible objects flow. The insight from the present study can also help for better understanding the compaction and packaging of quasi-1D semiflexible objects [48–50] and can be used as a guide to design the micro/nano-structure of new materials.

Materials and methods

Vane rheometer

A rheometer measuring head (Anton-Paar DSR 502, Austria, Graz) was mounted on a vertically moving frame with a digimatic indicator (ID-H Series, Mitutoyo, The Netherlands, Veenendaal) to accurately adjust the height of the probe. A custom made cup, consisting of a 250 mL glass beaker roughened with bead chains, was attached to the bottom plate. A four-blade vane (ST22-4V-40, Serial No.: 18180, Anton-Paar, Austria, Graz) of 22 mm diameter and 40 mm height was used. To record the movements at the top surface, a GoPro Hero 4 Silver camera (GoPro, U.S., San Mateo) was used with a frame rate of 25 frames/s. The probe was first inserted into the cup and secured by hand while loading the sample. To avoid exceeding the maximum torque that the rheometer could apply, the bead chains or spaghetti were loaded into the cup up to 2 cm and 4 cm height, respectively. After loading the spaghetti samples, they were gently pushed downwards without being fractured. For experiments with spaghetti a lid, made of a low-density polyethylene petri dish and secured between an additional layer of chains on the beaker wall, was used to prevent the samples from ascending above the probe. In case of bead chains, the beaker was vibrated for 2 mins on a Vortex-Genie 2 test tube shaker (Scientific Industries, U.S., Bohemia) to reach the maximum possible packing fraction. Next, the probe was connected to the rheometer head and pre-sheared at 1 Hz frequency and 63 mrad rotation amplitude for 4 mins. Finally, the oscillatory shear tests were carried out at 0.1 Hz frequency and over a rotation amplitude range limited by the maximum torque that the rheometer could apply ($\phi_0 \leq 0.6$ rad for bead chains and $\phi_0 \leq 1.9$ rad for spaghetti).

Bead chains

Stainless steel granular bead chains (Grootspul, The Netherlands, Driebergen) were used with a bead diameter of 2.4 mm, a maximum distance of 2.8 mm between the centers of neighboring beads, and a maximum turning angle of 40° , resulting in a minimum loop circumference of 9 beads. The bead chains were cut into lengths of 3, 9, and 45 beads, as well as monomers. Sunflower oil (Vandemoortele Nederland BV, The Netherlands, Zeewolde) was used as a lubricant to reduce the friction coefficient to $\mu \approx 0.2$; the chains were coated by shaking them for 10 mins in plastic containers using 0.02 mL of oil per gram of beads.

Cooked spaghetti

Dehydrated dry spaghetti (Jumbo Spaghetti Naturel, The Netherlands, Veghel) were cut into lengths of 1.0, 3.0, 9.0 and 15.0 cm. Excess starch was cleaned by submerging the spaghetti in cold tap water for 10 s twice, while gently stirring using a spatula. The samples were subsequently boiled for 9 mins and cooled in a sieve using running cold tap water. The majority of the water was drained. Next, sunflower oil (Vandemoortele Nederland BV, The Netherlands, Zeewolde) was used as a lubricant; the samples were coated using 0.02 mL oil per gram of boiled spaghetti by stirring and subsequent shaking by hand for 5 mins in a closed plastic container. Due to swelling of the spaghetti during cooking, the final strand lengths were 1.3 ± 0.2 , 3.5 ± 0.1 , 12.3 ± 0.2 and 19.6 ± 0.2 cm. The spaghetti samples were stored in closed containers at room temperature and measured within eight hours after preparation.

Image processing

Particle image velocimetry (PIV) was performed using PIVlab 2.55 plugin [51], a tool developed for MATLAB R2019b (MathWorks, U.S., Natick). The settings for PIVlab were used as described in [52]. Four passes were applied for PIV estimation with the first being approximately four times and the last about a half of the

bead diameter. The images were calibrated for time and space using the time between successive frames and the width of the beaker at the sample surface, respectively.

Simulation method

Simulations of bead chains were performed using the contact dynamics (CD) method [36, 37]. To construct the chains, spherical rigid beads of diameter d were connected to each other by imposing an upper bound on the distance $d+\ell$ between the centers of neighboring beads, with ℓ being the gap between the surfaces of the two beads. The maximum gap size ℓ_{\max} varied within $0 \leq \ell_{\max} < d/2$ in different simulations; thus, the gap between beads on the same chain was always smaller than the bead radius to ensure that the neighboring beads remain so close to each other that the imaginary bonds between the beads of different chains never touch. To tune the flexibility of the chains, the angle θ between the lines connecting the centers of successive bead pairs on the chain was limited to an upper bound θ_{\max} ($\theta_{\max} \in \{20^\circ, 30^\circ, 40^\circ, 50^\circ, 60^\circ, 70^\circ\}$ in different simulations). The bead chain length was varied from $N=1$ (individual beads) to $N=100$.

A layer of beads was fixed at the lateral and bottom walls of a cylindrical container of height $20d$ to provide rough boundaries. The inner diameter of the container was $29d$ and a rotating four-blade vane of diameter $9d$ was constructed by touching rigid beads. The container was first loaded with chains of equal size and relaxed into equilibrium under gravity. Next, the vane was rotated in an oscillatory fashion with 1Hz frequency and $\pi/50$ rad amplitude for 240 s. The oscillatory shear tests were carried out at 0.1Hz frequency and for different amplitudes. The total torque exerted on the vane was measured after each $\Delta\phi=10^{-3}$ rad change in the deflection angle.

-
- [1] Hansell, M. *Animal Architecture* (Oxford Animal Biology Series, Oxford, 2005).
- [2] Verhille, G., Moulinet, S., Vandenberghe, N., Adda-Bedia, M. & Gal, P. L. Structure and mechanics of aegagropilae fiber network. *Proc. Natl. Acad. Sci. USA* **114**, 4607–4612 (2017).
- [3] Weiner, N., Bhosale, Y., Gazzola, M. & King, H. Mechanics of randomly packed filaments—the “bird nest” as meta-material. *J. Appl. Phys.* **127**, 050902 (2020).
- [4] Brown, E., Nasto, A., Athanassiadis, A. G. & Jaeger, H. M. Strain stiffening in random packings of entangled granular chains. *Phys. Rev. Lett.* **108**, 108302 (2012).
- [5] Dumont, D., Houze, M., Rambach, P., Salez, T., Patinet, S. & Damman, P. Emergent strain stiffening in interlocked granular chains. *Phys. Rev. Lett.* **120**, 088001 (2018).
- [6] Zou, L. N., Cheng, X., Rivers, M. L., Jaeger, H. M. & Nagel, S. R. The packing of granular polymer chains. *Science* **326**, 408–410 (2009).
- [7] Gómez, L. R., Garcia, N. A. & Pöschel, T. Packing structure of semiflexible rings. *Proc. Natl. Acad. Sci. USA* **117**, 3382–3387 (2020).
- [8] Soh, B. W., Gengaro, I. R., Klotz, A. R. & Doyle, P. S. Self-entanglement of a tumbled circular chain. *Phys. Rev. Res.* **1**, 033194 (2019).
- [9] Ben-Naim, E., Daya, Z. A., Vorobieff, P. & Ecke, R. E. Knots and random walks in vibrated granular chains. *Phys. Rev. Lett.* **86**, 1414–1417 (2001).
- [10] Lopatina, L. M., Olson Reichhardt, C. J. & Reichhardt, C. Jamming in granular polymers. *Phys. Rev. E* **84**, 011303 (2011).
- [11] Sarate, P. S., Murthy, T. G. & Sharma, P. Column to pile transition in quasi-static deposition of granular chains. *Soft Matter* **18**, 2054–2059 (2022).
- [12] Safford, K., Kantor, Y., Kardar, M. & Kudrolli, A. Structure and dynamics of vibrated granular chains: Comparison to equilibrium polymers. *Phys. Rev. E* **79**, 061304 (2009).
- [13] Samadi Taheri, F., Fazli, H., Doi, M. & Habibi, M. Granular chain escape from a pore in a wall in the presence of particles on one side: a comparison to polymer translocation. *Soft Matter* **14**, 5420–5427 (2018).
- [14] Sunami, H., Shimizu, Y., Futenma, N., Denda, J., Nakasone, H., Yokota, S., Kishimoto, H., Makita, M. & Nishikawa, Y. Rapid stem cell extraction and culture device for regenerative therapy using biodegradable non-woven fabrics with strongly oriented fibers. *Adv. Mater. Interfaces* **9**, 2101776 (2022).
- [15] Hu, J., Meng, H., Li, G. & Ibekwe, S. I. A review of stimuli-responsive polymers for smart textile applications. *Smart Mater. Struct.* **21**, 053001 (2012).
- [16] Yun, Y. J., Hong, W. G., Kim, W.-J., Jun, Y. & Kim, B. H. A novel method for applying reduced graphene oxide directly to electronic textiles from yarns to fabrics. *Adv. Mater.* **25**, 5701–5705 (2013).
- [17] Poincloux, S., Adda-Bedia, M. & Lechenault, F. Geometry and elasticity of a knitted fabric. *Phys. Rev. X* **8**, 021075 (2018).
- [18] Haines, C. S., Li, N., Spinks, G. M., Aliev, A. E., Di, J. & Baughman, R. H. New twist on artificial muscles.

- Proc. Natl. Acad. Sci. USA* **113**, 11709–11716 (2016).
- [19] Mueth, D. M., Debregeas, G. F., Karczmar, G. S., Eng, P. J., Nagel, S. R. & Jaeger, H. M. Signatures of granular microstructure in dense shear flows. *Nature* **406**, 385 (2000).
- [20] Losert, W., Bocquet, L., Lubensky, T. C. & Gollub, J. P. Particle dynamics in sheared granular matter. *Phys. Rev. Lett.* **85**, 1428–1431 (2000).
- [21] Shaebani, M. R., Török, J., Maleki, M., Madani, M., Harrington, M., Rice, A. & Losert, W. Gravity governs shear localization in confined dense granular flows. *Phys. Rev. Lett.* **127**, 278003 (2021).
- [22] Fenistein, D. & van Hecke, M. Wide shear zones in granular bulk flow. *Nature* **425**, 256 (2003).
- [23] Unger, T., Török, J., Kertész, J. & Wolf, D. E. Shear band formation in granular media as a variational problem. *Phys. Rev. Lett.* **92**, 214301 (2004).
- [24] R. Moosavi et. al. Coexistence and transition between shear zones in slow granular flows. *Phys. Rev. Lett.* **111**, 148301 (2013).
- [25] Aktas, B., Narang, Y. S., Vasios, N., Bertoldi, K. & Howe, R. D. A modeling framework for jamming structures. *Adv. Funct. Mater.* **31**, 2007554 (2021).
- [26] Mirzaali, M. J., Habibi, M., Janbaz, S., Vergani, L. & Zadpoor, A. A. Crumpling-based soft metamaterials: the effects of sheet pore size and porosity. *Sci. Rep.* **7**, 13028 (2017).
- [27] Kamani, K., Donley, G. J. & Rogers, S. A. Unification of the rheological physics of yield stress fluids. *Phys. Rev. Lett.* **126**, 218002 (2021).
- [28] Matoz-Fernandez, D. A., Agoritsas, E., Barrat, J. L., Bertin, E. & Martens, K. Nonlinear rheology in a model biological tissue. *Phys. Rev. Lett.* **118**, 158105 (2017).
- [29] Rogers, S. Large amplitude oscillatory shear: Simple to describe, hard to interpret. *Phys. Today* **71**, 34–40 (2018).
- [30] Baggioli, M., Grieninger, S. & Soltanpanahi, H. Non-linear oscillatory shear tests in viscoelastic holography. *Phys. Rev. Lett.* **124**, 081601 (2020).
- [31] Tapadia, P., Ravindranath, S. & Wang, S. Q. Banding in entangled polymer fluids under oscillatory shearing. *Phys. Rev. Lett.* **96**, 196001 (2006).
- [32] Regev, I. & Reichhardt, C. Rheology and shear band suppression in particle and chain mixtures. *Phys. Rev. E* **87**, 020201 (2013).
- [33] Shaebani, M. R., Jose, R., Santen, L., Stankevics, L. & Lautenschläger, F. Persistence-speed coupling enhances the search efficiency of migrating immune cells. *Phys. Rev. Lett.* **125**, 268102 (2020).
- [34] Doi, M. & Edwards, S. F. *The Theory of Polymer Dynamics* (Oxford University Press, Oxford, 1986).
- [35] Mortazavi, F., Habibi, M. & Nedaaee Oskoe, E. Translocation of a granular chain in a horizontally vibrated sawtooth channel. *Eur. Phys. J. E* **39**, 93 (2016).
- [36] Z. Shojaee et. al. An adaptive hierarchical domain decomposition method for parallel contact dynamics simulations of granular materials. *J. Comput. Phys.* **231**, 612–628 (2012).
- [37] Jean, M. The non-smooth contact dynamics method. *Comput. Methods Appl. Mech. Eng.* **177**, 235–257 (1999).
- [38] Shaebani, M. R., Unger, T. & Kertész, J. Generation of homogeneous granular packings: contact dynamics simulations at constant pressure using fully periodic boundaries. *Int. J. Mod. Phys. C* **20**, 847–867 (2009).
- [39] Toiya, M., Stambaugh, J. & Losert, W. Transient and oscillatory granular shear flow. *Phys. Rev. Lett.* **93**, 088001 (2004).
- [40] Shaebani, M. R., Unger, T. & Kertész, J. Unjamming due to local perturbations in granular packings with and without gravity. *Phys. Rev. E* **78**, 011308 (2008).
- [41] Unger, T., Kertész, J. & Wolf, D. E. Force indeterminacy in the jammed state of hard disks. *Phys. Rev. Lett.* **94**, 178001 (2005).
- [42] Shaebani, M. R., Unger, T. & Kertész, J. Extent of force indeterminacy in packings of frictional rigid disks. *Phys. Rev. E* **79**, 052302 (2009).
- [43] Ward, A., Hilitski, F., Schwenger, W., Welch, D., Lau, A. W. C., Vitelli, V., Mahadevan, L. & Dogic, Z. Solid friction between soft filaments. *Nat. Mater.* **14**, 583 (2015).
- [44] Ewoldt, R. H., Hosoi, A. E. & McKinley, G. H. New measures for characterizing nonlinear viscoelasticity in large amplitude oscillatory shear. *J. Rheol.* **52**, 1427–1458 (2008).
- [45] Goldenberg, C. & Goldhirsch, I. Friction enhances elasticity in granular solids. *Nature* **435**, 188–191 (2005).
- [46] Shaebani, M. R., Unger, T. & Kertész, J. Unjamming of granular packings due to local perturbations: Stability and decay of displacements. *Phys. Rev. E* **76**, 030301 (2007).
- [47] Negi, V. & Picu, R. C. Tensile behavior of non-crosslinked networks of athermal fibers in the presence of entanglements and friction. *Soft Matter* **17**, 10186–10197 (2021).
- [48] Stoop, N., Najafi, J., Wittel, F. K., Habibi, M. & Herrmann, H. J. Packing of elastic wires in spherical cavities. *Phys. Rev. Lett.* **106**, 214102 (2011).
- [49] Shaebani, M. R., Najafi, J., Farnudi, A., Bonn, D. & Habibi, M. Compaction of quasi-one-dimensional elastoplastic materials. *Nat. Commun.* **8**, 15568 (2017).
- [50] Vetter, R., Wittel, F. K. & Herrmann, H. J. Morphogenesis of filaments growing in flexible confinements. *Nat. Commun.* **5**, 4437 (2014).
- [51] Thielicke, W. & Stamhuis, E. J. Pivlab - towards user-friendly, affordable and accurate digital particle image velocimetry in matlab. *J. Open Res. Softw.* **2**, 1–10 (2014).
- [52] Sarno, L., Tai, Y.-C., Carravetta, A., Martino, R., Nicolina Papa, M. & Kuo, C.-Y. Challenges and improvements in applying a particle image velocimetry (piv) approach to granular flows. *J. Phys. Conf. Ser.* **1249**, 012011 (2019).

Acknowledgments

M.H. acknowledges funding from the Netherlands Organization for Scientific Research through NWO-VIDI grant No. 680-47-548/983. M.R.S. acknowledges support by the Deutsche Forschungsgemeinschaft (DFG) through Collaborative Research Center SFB 1027 and by the Young Investigator Grant of the Saarland University, Grant No. 7410110401.

Author contributions

M.H. designed the research; M.H. and G.G.-R. planned the experiments; G.G.-R. and S.Z. carried out the experiments; G.G.-R., S.Z., M.H., and M.R.S. analyzed the data; All authors contributed to the interpretation of the results; M.R.S. designed and performed the simulations and wrote the manuscript. M.R.S. and G.G.-R. equally contributed to this work. Correspondence and requests for materials should be addressed to M.H. (mehdi.habibi@wur.nl) or M. R. S. (shaebani@lusi.uni-sb.de).

Competing interests

The authors declare that they have no competing interests.

Data and materials availability

All data needed to evaluate the conclusions in the paper are present in the paper. Additional data related to this paper may be requested from the authors.

Supplementary materials

Movie S1. Examples of oscillatory shear experiments with chain length $N=1$ or 9 and rotation amplitude $\phi_c = 0.063$ or 0.632 rad.